Phonon-induced breakdown of Thouless pumping in the Rice-Mele-Holstein model

Suman Mondal, Eric Bertok, and Fabian Heidrich-Meisner
Institut für Theoretische Physik, Georg-August-Universität Göttingen, D-37077 Göttingen, Germany

(Received 16 September 2022; revised 14 November 2022; accepted 22 November 2022; published 12 December 2022)

Adiabatic and periodic variation of the lattice parameters can make it possible to transport charge through a system even without net external electric or magnetic fields, known as Thouless charge pumping. The amount of charge pumped in a cycle is quantized and entirely determined by the system's topology, which is robust against perturbations such as disorder and interactions. However, coupling to the environment may play a vital role in topological transport in many-body systems. We study the topological Thouless pumping, where the charge carriers interact with local optical phonons. The semiclassical multitrajectory Ehrenfest method is employed to treat the phonon trajectories classically and charge carriers quantum mechanically. We find a breakdown of the quantized charge transport in the presence of phonons. It happens for any finite electron-phonon coupling strength at the resonance condition when the pumping frequency matches the phonon frequency, and it takes finite phonon coupling strength away from the resonance. Moreover, there exist parameter regimes with non-quantized negative and positive charge transport. The modified effective pumping path due to electron-phonon coupling accurately explains the underlying physics. In the large coupling regime where the pumping disappears, the phonons are found to eliminate the staggering of the on-site potentials, which is necessary for the pumping protocol. Finally, we present a stability diagram of quantized pumping as a function of the time period of pumping and phonon coupling strength.

DOI: 10.1103/PhysRevB.106.235118

I. INTRODUCTION

A Thouless charge pump, on a fundamental level, is a one-dimensional dynamic equivalent to the quantum Hall effect. The robust transport of quantized charge in an adiabatic pump cycle, defined by periodic variation of lattice parameters, was first introduced almost four decades ago by Thouless [1]. Recently, this fundamental physical phenomenon has been experimentally demonstrated in a variety of quantum systems, such as ultracold atoms in optical lattices and photonic lattices [2–8]. The robustness of quantization is attributed to the underlying topological protection, which is not altered under small perturbations such as disorder and interaction. In recent years, studying the effect of disorder, different kinds of interaction and nonlinearity have been a topic of immense interest [9–26]. On the experimental front, topological Thouless pumping has been studied in the presence of disorder [27] and strongly correlated regimes [28]. In the attempt to extend the concept of topology to finite temperature and open quantum systems [29–39], Thouless charge pumping has also been studied in these contexts [35,37,38].

The robustness of the topological properties of a system against an open environment is important to study since quantum systems, in general, always interact with the environment. There are several studies that deal with open topological systems that investigate the density matrix by solving the master equation [40–42]. We study a closed system where the topological system is a subsystem, and the rest of the system acts as an environment. The dynamics, in this case, is unitary. In our case, we consider an ensemble of uncoupled classical harmonic oscillators as the environment. In the solid-state context, this realizes Einstein phonons. Our primary goal is to study the breakdown of topology in the presence of the coupling to the environment. Note that the interplay between the topology and the phonon has been studied before for different systems such as quantum Hall and systems with Majorana fermions [43–46].

One of the very crucial aspects of many-body physics is the interaction with the lattice degree of freedom. Phonons arise naturally as the lattice vibrations at any finite temperature in a real material. The electron-phonon (*e*-ph) coupling can cause instabilities in the metallic state, leading to a plethora of important phenomena, e.g., polaron formation [47], superconductivity, and charge density waves [48–53]. The phononic degrees of freedom show a drastic effect on the dynamical properties as a result of the exchange of energies between the electronic and phononic sectors [54–61]. A great deal of research has been done to analyze the effect of phonons on the dynamics of the charge density wave and Mott phases [54,55,57,59,60], Bloch oscillations [58,61], the equilibration of excited charge carriers [56], and thermalization [62]. The formation of and evolution of polarons have also been extensively studied [63–68]. One theoretical model that represents such strongly correlated *e*-ph systems where the electrons are coupled to the local phonons is the Holstein model [69].

In this work, we analyze the stability of the topology where the system is coupled to a phononic environment. The transport of charge in Thouless charge pumping is studied using the Rice-Mele model [70] subjected to optical phonons, which we dub the Rice-Mele-Holstein model. We use the semiclassical

method known as multitrajectory Ehrenfest (MTE) [71–74] and time evolve the initial state with the phonons in the ground state. The trajectory-based mixed quantum-classical dynamics was traditionally introduced to study electron-nuclear systems, which works best in the adiabatic limit of phonons with oscillator frequencies smaller than the electronic bandwidth [71–74].

In our analysis with the MTE method, we see a breakdown of topological charge pumping (TCP) in the presence of phonons. At resonance, when the phonon frequency and pumping frequency are equal, the TCP breaks for any finite value of e-ph coupling. In the minimal e-ph coupling limit, the TCP eventually disappears at the higher pump cycles. It takes a finite e-ph interaction before the TCP breaks down away from the resonance. In other words, the TCP is stable at sufficiently finite e-ph coupling in this case. The breakdown of TCP is complimented with a gap closing in the spectrum of the instantaneous effective Hamiltonian during the evolution.

Apart from quantized pumping, parameter regimes where nonquantized positive and negative pumping happen exist. The analysis of an effective pumping path very efficiently explains different aspects, such as the direction of pumping and breakdown of pumping. Here, the effective pumping path is the modified Rice-Mele path due to the coupling between the phonon position, which changes dynamically, and on-site electron density. The direction of winding around the origin and the origin crossing by the effective pumping path determine the direction and breakdown of pumping, respectively. We present a stability diagram for the quantized pumping as a function of e-ph coupling strength and pumping period. For a fixed e-ph coupling (small), the diagram displays a signature of reentrant TCP as a function of time period of pumping; that is, the quantization of the pumped charge reappears after losing quantization near the resonance.

In summary, the main findings of this paper are as follows: (i) We see a robust quantized pumping with finite electron-phonon coupling for a wide range of parameters which eventually disappears at large electron-phonon coupling. (ii) A resonance effect exists where the quantized pumping breaks down for any finite electron-phonon coupling. (iii) The system exhibits a phenomenon of negative pumping, where the charge flows opposite to the driving, in some parameter regime, but this occurs outside the quantized regime.

The rest of this paper is organized as follows. In Sec. II, we review the model and the methods used in this work. There we introduce the Rice-Mele model that defines the Thouless pumping protocol and extend it with a Holstein-like coupling to local phonons. Next, we briefly explain the trajectory-based semiclassical MTE method, which is employed to perform the time evolution, and describe the observables used to analyze the physics. The concept of an effective pumping path is introduced at the end of that section. The discussion of results starts in Sec. III. In that section, we explain the breakdown of TCP and nonquantized pumping in terms of the pumped charge, effective pumping paths, and instantaneous eigenvalue spectra at resonance. In Sec. IV, we do an analysis similar to that in Sec. III when the system is out of resonance. Then, we describe the stability diagram obtained as a function of the time period of pumping and e-ph coupling strength in Sec. V. Finally, we draw conclusions in Sec. VI.

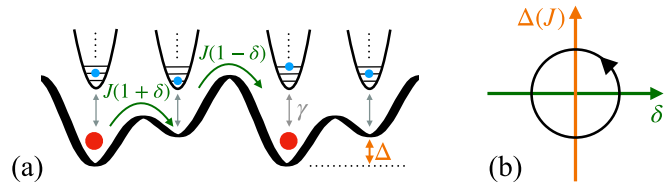

FIG. 1. A pictorial representation of system parameters is shown. (a) Potential landscape at a specific point in time during a pump cycle that determines the hopping dimerization δ and staggered potential Δ. The phonon bath at every site is represented by the harmonic oscillator potential, coupled to the site with strength γ. (b) The pumping protocol. If the system parameter winds around the origin adiabatically, quantized pumping is expected for $\gamma = 0$.

II. MODEL AND METHOD

A. The Rice-Mele model

The Thouless pumping protocol can be defined by the Rice-Mele model [70], a time-dependent Hamiltonian with a time t varying superlattice potential, given by

$$\hat{H}_{\mathrm{RM}}(t) = \sum_{i=1}^{L} -J(1+(-1)^i\delta(t))(\hat{c}_i^\dagger \hat{c}_{i+1} + \mathrm{H.c.}) + \sum_{i=1}^{L}(-1)^i \frac{\Delta(t)}{2}\hat{n}_i, \tag{1}$$

that changes the hopping amplitude and on-site potential with time. Here, $\hat{c}_i$ ($\hat{c}_i^\dagger$) and $\hat{n}_i$ are the fermionic (say, electrons) annihilation (creation) and on-site number operators, respectively, at site i in a system consisting of L sites. $\delta(t)$ and $\Delta(t)$ are the hopping dimerization and on-site staggered potential, respectively, that vary with t,

$$\delta(t) = A_\delta \sin\left(\frac{2\pi t}{T} + \phi\right), \qquad \Delta(t) = A_\Delta \cos\left(\frac{2\pi t}{T} + \phi\right), \tag{2}$$

where T is the pumping period and $\tau = t/T$ can be considered the pumping parameter. ϕ is an offset of the pumping protocol which is considered to be $\phi = \pi/2$ in this work, realizing $\Delta(t) = 0$ and $\delta(t) > 0$ at $t = 0$, known as the Su-Schrieffer-Heeger [75] limit. An example of the potential landscape is shown in Fig. 1(a) for some t which demonstrates the hopping dimerization and staggered potential. The unit cell of the lattice consists of two sublattices A and B, implying the existence of two bands. For finite A_δ and A_Δ, the band gap is always finite for all t at half filling, and t defines a pumping trajectory that winds around the gap-closing point at $\Delta = \delta = 0$, as shown in Fig. 1(b). For an adiabatic change of τ (large enough T), the topological nature ensures the pumping of a quantized amount of charge Q in a pump cycle. We can quantify the total number of charges pumped during the time evolution by integrating the current at a particular bond between two sites (the first odd bond is considered in our results) as

$$Q(t) = \int_0^t I_{i,i+1}(t)dt, \tag{3}$$

where

$$I_{i,i+1}(t) = -2\mathrm{Im}J_{i,i+1}(t)\langle\Psi(t)|\hat{c}^{\dagger}_{i+1}\hat{c}_i|\Psi(t)\rangle \tag{4}$$

is the current at time t at the bond between sites i and $i+1$, which has a time-dependent hopping amplitude $J_{i,i+1} = J[1 + (-1)^i\delta(t)]$.

B. The Rice-Mele-Holstein model

The coupling between charge carriers (electrons) and optical phonons extends the Rice-Mele model [Eq. (15)] to the Rice-Mele-Holstein model. The Holstein-like coupling is defined by the dispersionless phonons, also known as Einstein phonons, coupled to the local electronic state, given by

$$\hat{H}(t) = \hat{H}_{\mathrm{RM}}(t) + \hat{H}_{\mathrm{ph}} + \hat{H}_{e\text{-ph}}. \tag{5}$$

Here, $\hat{H}_{\mathrm{ph}}$ and $\hat{H}_{e\text{-ph}}$ are the phonon and e-ph coupling parts of the Hamiltonian, which are given by

$$\hat{H}_{\mathrm{ph}} = \hbar\omega\sum_{i=1}^{L}\hat{b}^{\dagger}_i\hat{b}_i \tag{6}$$

and

$$\hat{H}_{e\text{-ph}} = -\gamma\sum_{i=1}^{L}(\hat{b}^{\dagger}_i + \hat{b}_i)\hat{n}_i. \tag{7}$$

$\hat{b}_i$ ($\hat{b}^{\dagger}_i$) are the bosonic annihilation (creation) operators of the phonons at site i. ω and γ are the phonon frequency and e-ph coupling strength, respectively. The e-ph coupling is shown in Fig. 1(a), which illustrates how the phonon bath is coupled to a site.

The Thouless pump in this scenario can be studied with the real-time evolution of an initial state $|\Psi(0)\rangle$ under the influence of a time-dependent Hamiltonian $\hat{H}(t)$. In our calculation we consider $|\Psi(0)\rangle$ to be

$$|\Psi(0)\rangle = |\Psi_e(0)\rangle|\Psi_{\mathrm{ph}}(0)\rangle, \tag{8}$$

where $|\Psi_e(0)\rangle$ is the ground state of $\hat{H}_{\mathrm{RM}}(0)$ at half filling and $|\Psi_{\mathrm{ph}}(0)\rangle = \prod_{i=1}^{L}|\psi^i_{\mathrm{ph}}(0)\rangle$ represents the ground state of $\hat{H}_{\mathrm{ph}}$ where at each site i, phonons are in the ground state $|\psi^i_{\mathrm{ph}}(0)\rangle$ of each individual oscillator.

C. Multitrajectory Ehrenfest method

In principle, the problem can be simulated using numerical methods such as exact diagonalization, Lanczos time evolution, and the time-dependent density matrix renormalization group (tDMRG) methods to capture the exact dynamics for relatively smaller systems [59,76–79], although not straightforwardly in the adiabatic regime. In this work, we employ a semiclassical approximate approach called the multitrajectory Ehrenfest method, which treats phonons classically and averages over independent trajectories. Since we are primarily interested in the regime of small phonon frequencies where we expect the most immediate effect on the pump, we choose MTE, which is efficient and reliable in this regime [74]. This method simplifies our problem to such an extent that it can be solved using the single-particle eigenstates of the Hamiltonian. The classical trajectory-based MTE method is described extensively in Ref. [74], and in the following, we describe it briefly. To apply the MTE method the phononic operators are represented in real space via $\hat{b}^{\dagger}_i = \sqrt{\frac{m\omega}{2\hbar}}(\hat{x}_i + \frac{\hat{p}_i}{m\omega})$, and by using the natural length scale for the harmonic oscillators $l_0 = \sqrt{\frac{\hbar}{m\omega}} = 1$ and $\hbar = 1$, we get

$$\hat{H}_{\mathrm{ph}} = \frac{\omega}{2}\sum_{i=1}^{L}\left(\hat{x}^2_i + \hat{p}^2_i\right), \tag{9}$$

ignoring the constant term $-\omega L/2$, and

$$\hat{H}_{e\text{-ph}} = -\sqrt{2}\gamma\sum_{i=1}^{L}\hat{x}_i\hat{n}_i. \tag{10}$$

Under the MTE approximation, $|\Psi(0)\rangle$ can now be evolved by initializing the different sets of phonon coordinates $\{x_i(0), p_i(0)\}$, which define different independent trajectories. Here, $\{x_i(0), p_i(0)\}$ are randomly drawn from the distribution given by the Wigner function W_0 centered around $\langle x\rangle = 0$ and $\langle p\rangle = 0$. W_0 is the phase space representation of the harmonic oscillator ground state $|\psi_{\mathrm{ph}}(0)\rangle$,

$$W_0 = \frac{1}{\pi}e^{-(x-\langle x\rangle)^2-(p-\langle p\rangle)^2}. \tag{11}$$

The electronic wave function $|\Psi_e(0)\rangle$ evolves under the Hamiltonian

$$\hat{H}_{\mathrm{el}} = \hat{H}_{\mathrm{RM}}(t) - \sqrt{2}\gamma\sum_{i=1}^{L}x_i(t)\hat{n}_i, \tag{12}$$

which depends on only the dynamical position $x_i(t)$ of the phonons, $i\frac{\partial}{\partial t}|\Psi_e\rangle = \hat{H}_{\mathrm{el}}|\Psi_e\rangle$. The phonon coordinates simultaneously propagate in phase space via the Newtonian mechanics under the influence of the classical Hamiltonian,

$$H_{\mathrm{cl}} = \frac{\omega}{2}\sum_{i=1}^{L}\left(x^2_i + p^2_i\right) - \sqrt{2}\gamma\sum_{i=1}^{L}x_i\langle\Psi_e(t)|\hat{n}_i|\Psi_e(t)\rangle, \tag{13}$$

as $\dot{x}_i = \frac{\partial H_{\mathrm{cl}}}{\partial p_i}$, $\dot{p}_i = -\frac{\partial H_{\mathrm{cl}}}{\partial x_i}$.

The expectation value of any observable $\hat{O}$ can be calculated by averaging over all the trajectories as

$$\langle\hat{O}(t)\rangle = \frac{1}{N_{\mathrm{traj}}}\sum_{i=1}^{N_{\mathrm{traj}}}\langle\Psi_i(t)|\hat{O}|\Psi_i(t)\rangle, \tag{14}$$

where N_{traj} is the number of trajectories and $|\Psi_i(t)\rangle$ is the time-evolved initial electronic wave function $|\Psi_e(0)\rangle$ at time t for the ith trajectory. In the following section, we present the results where we always consider $J = 1$, making all the parameters unitless, and express everything in units of J and $A_\Delta = 4A_\delta = 3$, defining a closed path around the gap-closing point at the origin in Fig. 1(b). Considering the limitations of the multitrajectory Ehrenfest method as mentioned above, we take $\omega = 0.1J$, which is small compared to J. In our numerical simulation, we always start the pumping protocol from a short negative time ($\frac{-T}{16J}$) without any phonon coupling and drive it slowly (compared to the actual pumping speed) to $t = 0$, where we quench γ. The slow drive before $t = 0$ leads to a smoother pumping during the execution of the pump cycles [13].

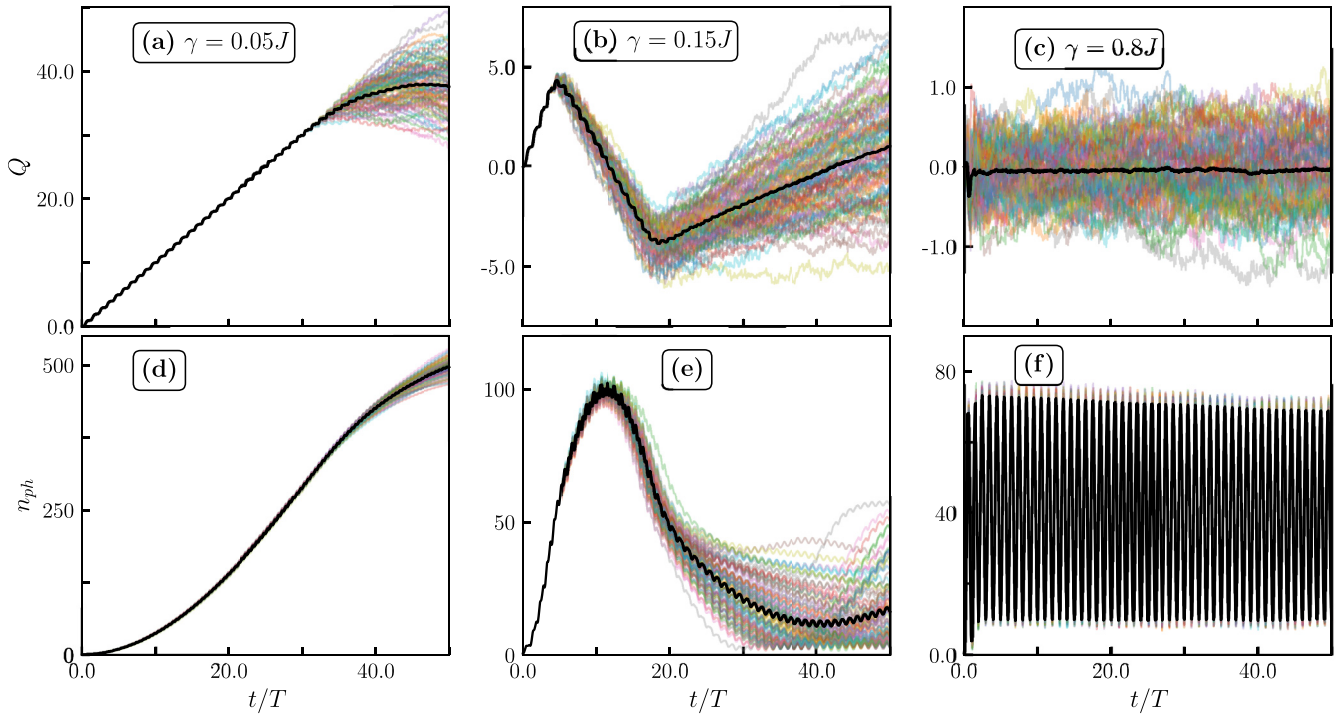

FIG. 2. Observables obtained in the time evolution in 50 pump cycles at resonance for $N_{\text{traj}} = 100$ and $\omega = 0.1J$ with $T = 2\pi/\omega$. $Q(t)$ for all the trajectories (lines with transparent colors) and the trajectory average $Q(t)$ (black line) are shown in (a)–(c) for $\gamma = 0.05J$, $0.15J$, and $0.8J$, respectively. Similar to what we did in (a)–(c), we plot the phonon density n_{ph} in (d)–(f), respectively.

D. Effective pumping path

As mentioned above, the electronic dynamics is determined by $\hat{H}_{\text{el}}$ given in Eq. (12), which has two parts. The first part contains the control parameters [$\delta(t)$ and $\Delta(t)$], which defines a pumping path, as shown in Fig. 1(b). We expect the pumping to be positively or negatively quantized depending on the direction of the winding around the origin. The second part of $\hat{H}_{\text{el}}$ gives rise to another source of the on-site potential on top of the staggered $\Delta(t)$ by coupling $x_i(t)$ with the on-site $\hat{n}_i$. This additional source of the on-site potential may alter the effective staggered potential between the sublattices, leading to a deviation in the pumping path from the original one defined by $\hat{H}_{\text{RM}}$. We can quantify the effective pumping path in the $(\bar{\delta}, \bar{\Delta})$ plane, where $\bar{\delta}(t) = 2\delta(t)$ is the hopping dimerization, which is unchanged, and $\bar{\Delta}(t)$ is the trajectory and unit-cell-averaged potential difference between two sublattices, given by

$$\bar{\Delta}(t) = \Delta(t) - \frac{2\sqrt{2}\gamma}{LN_{\text{traj}}} \sum_{i=1}^{N_{\text{traj}}} \left(\sum_{j\in\text{even}}^{L} x_{i,j}(t) - \sum_{j\in\text{odd}}^{L} x_{i,j}(t) \right). \tag{15}$$

The following sections explain different phenomena, such as the breakdown of pumping and negative charge pumping using the effective pumping path. See Ref. [80].

III. RESONANCE CONDITION

While the Rice-Mele (RM) model shows robust TCP, the nonzero coupling ($\gamma > 0$) with the phonons gives rise to very rich physics. We begin the analysis with the condition when the phonon frequency matches the pumping frequency ($\omega = 2\pi/T$). ω is considered to be $0.1J$, which fixes the pumping period as $T = 2\pi/\omega$. In this scenario, the dynamics are adiabatic enough in the RM limit ($\gamma = 0$) with robust quantized pumping. The question is whether this TCP survives at finite γ. To answer this, we calculate different quantities during 50 pump cycles with different e-ph coupling strengths γ. In Figs. 2(a)–2(c) we plot $Q(t)$ for $\gamma = 0.05J$, $0.15J$, and $0.8J$, respectively, for 100 trajectories (transparent lines) where the average $Q(t)$ over the trajectories is represented by the opaque black line. We can see that even for a very small value of $\gamma = 0.05J$, the TCP breaks down in the later pump cycles. For $\gamma = 0.15J$, we see a complex behavior in pumping; it changes the direction of pumping after a few cycles. For a large value of $\gamma = 0.8J$, the pumping ceases to occur. We notice that when the quantization of pumping breaks down, $Q(t)$ becomes trajectory dependent and fluctuates around the average value. This behavior is similar to pumping in a disorder potential [21], which is not surprising since each trajectory is initialized with random initial values of $\{x_i(0), p_i(0)\}$.

Interestingly, the phonon excitation is very distinct in different parameter regimes of γ. Figures 2(d)–2(f) show the behaviors of the phonon density given by

$$n_{\text{ph}} = \frac{1}{L} \sum_{i=1} \left(\frac{x_i^2}{2} + \frac{p_i^2}{2} \right) \tag{16}$$

for the same parameters considered in Figs. 2(a)–2(c), respectively. Even though $Q(t)$ is quantized in the first few pump cycles for smaller γ [Figs. 2(a) and 2(b)], n_{ph} continuously in-

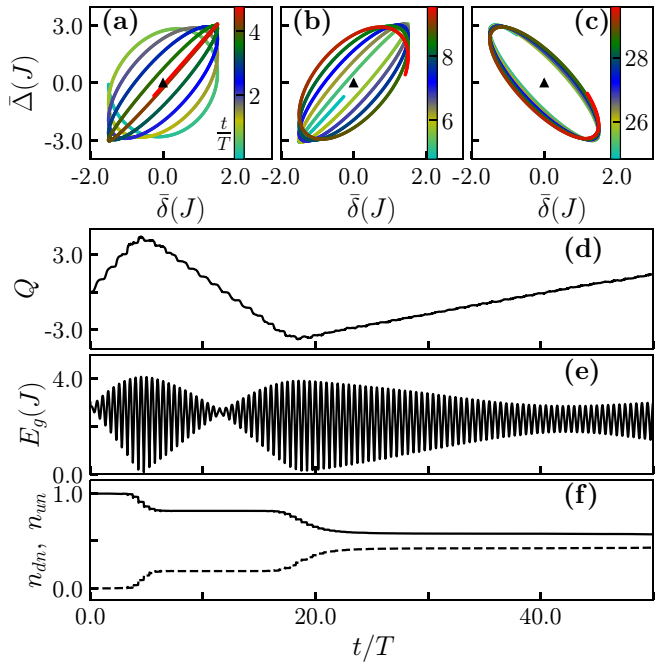

FIG. 3. Trajectory-averaged quantities are displayed here at resonance for $\gamma = 0.15J$, $\omega = 0.1J$, and $T = 2\pi/\omega$ with $N_{\text{traj}} = 100$. The trajectory-averaged effective pumping path is shown for three different time windows in (a)–(c), corresponding to Fig. 2(b), which is also shown in (d) for reference. The black triangles mark the origins where the gap should vanish. The direction of winding around the origin signifies the direction of pumping. $E_g(t)$ is shown in (e), and $n_{\text{dn}}(t)$ (solid line) and $n_{\text{up}}(t)$ (dashed line) are plotted in (f).

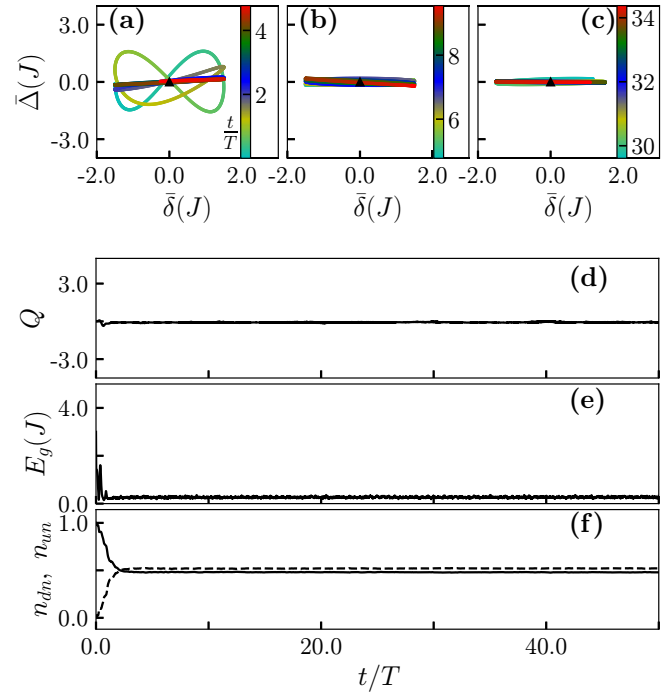

FIG. 4. Explanation of the breakdown of pumping at resonance for $\gamma = 0.8J$, $\omega = 0.1J$, and $T = 2\pi/\omega$. Different quantities are plotted after averaging over 100 trajectories. The effective pumping path is shown for three different time windows in (a)–(c), corresponding to Fig. 2(c), which is also shown in (d) for reference. The black triangles mark the origins where the gap should vanish. The frequent crossing of the origin by the effective pumping path signifies the breakdown of TCP. $E_g(t)$ is shown in (e), and $n_{\text{dn}}(t)$ (solid line) and $n_{\text{up}}(t)$ (dashed line) are plotted in (f).

creases, and eventually, the quantization of $Q(t)$ breaks down. When the pumping is completely suppressed [Fig. 2(c)], n_{ph} oscillates around a finite number with the frequency ω.

A. Negative charge pumping

The intricate evolution of $Q(t)$ seen in Fig. 2(b) is observed in a finite range of γ. To explain the multiple changes in pump direction, we analyze the effective pumping path. As discussed in Sec. II D, the instantaneous value of $x_i(t)$ can modify the effective pumping path. The pumping path defined by $(\bar{\delta}(t), \bar{\Delta}(t))$ is plotted for different time segments of the plot shown in Fig. 2(b), where the pumped charge is first positive (quantized) and then negative (nonquantized) and becomes positive (nonquantized) again with time, in Figs. 3(a)–3(c), respectively. The color bar represents the number of pump cycles t/T. We can see from Figs. 3(a)–3(c) that the path winds the origin (solid black triangle) first counterclockwise, then clockwise, and then in a counterclockwise direction again, respectively, which explains the direction of pumping. To check further why the quantization breaks down, we look into the trajectory-averaged gap in the spectrum of instantaneous $\hat{H}_{\text{el}}(t)$ given by

$$E_g(t) = E^{\text{el}}_{L/2+1}(t) - E^{\text{el}}_{L/2}(t), \tag{17}$$

where $\{E^{\text{el}}_{\alpha}(t)\}$ is the time-dependent energy spectrum of $\hat{H}_{\text{el}}(t)$ along with the occupancy of its lower (n_{dn}) and upper (n_{up}) bands with time. We can already see from Fig. 3(a) that, at the end of the first few cycles, the effective pumping path crosses the origin, where the gap in the spectrum of $\hat{H}_{\text{el}}(t)$ should close. $E_g(t)$ plotted in Fig. 3(d) exactly captures this gap closing. Until this point, n_{dn} (solid line) and n_{up} (dashed line) show that particles in $|\Psi(t)\rangle$ completely occupy the lower band, giving rise to the quantized pumping in this time segment. However, at $E_g = 0$, partial excitation to the upper band happens nonadiabatically, which can be inferred from the finite n_{up}. After this first gap-closing point, $E_g(t)$ becomes finite again, and since the effective pumping path winds in the opposite direction in this segment [Fig. 3(b)], it results in the negative charge pumping. The partial occupancy of the lower band breaks the quantization. A similar gap closing is detected again during the evolution, which populates the upper band further. The counterclockwise winding of the effective pumping path [Fig. 3(c)] suggests a positive pumping (nonquantized) since $E_g(t)$ is finite at later times.

B. Breakdown of pumping

To compare the previous situation with the case shown in Fig. 2(c) where the pumping is entirely absent, we carry out a similar analysis in Fig. 4. Here, the phonon coupling drastically perturbs the staggering nature of the potential, and the effective pumping path becomes flat along the $\bar{\delta}$ axis, which crosses the origin in every pump cycle [Figs. 4(a)–4(c)]. As a result, $Q(t)$ does not change with time. The vanishing $E_g(t)$, shown in Fig. 4(e), signifies nonadiabatic dynamics

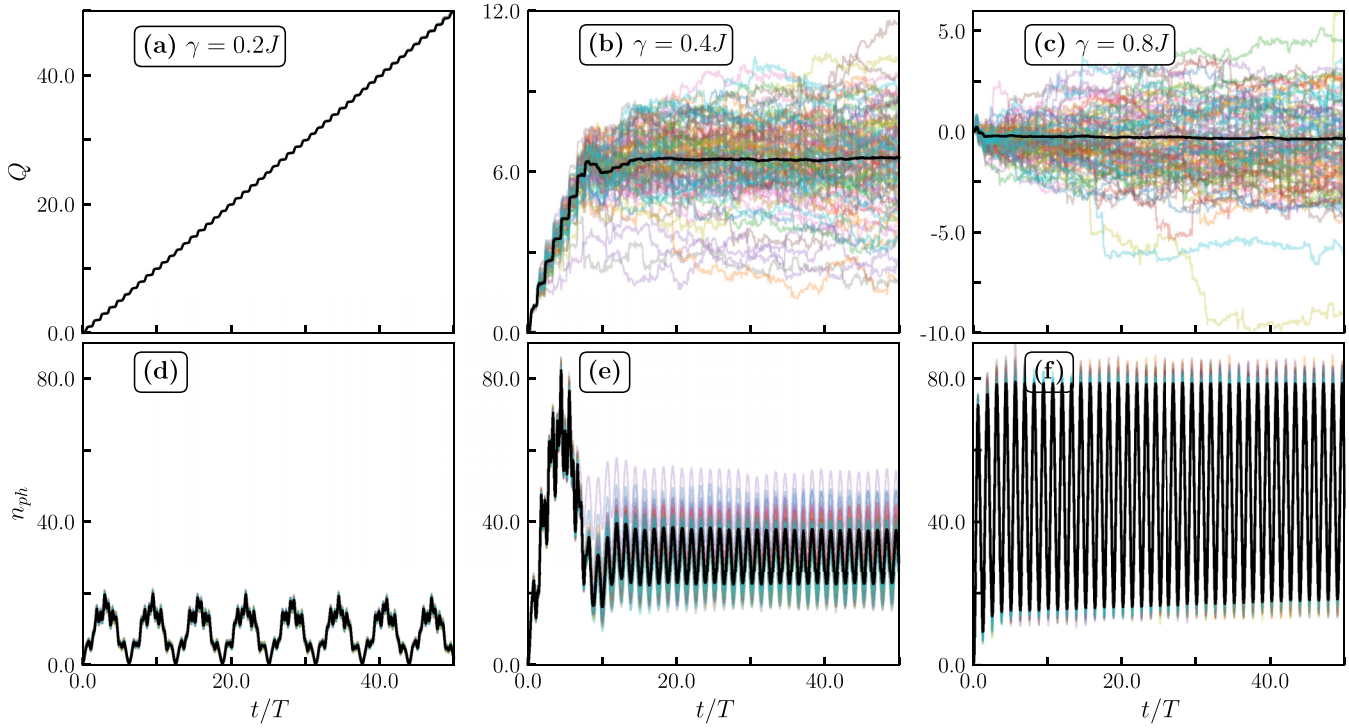

FIG. 5. Observables obtained in the time evolution in 50 pump cycles away from resonance for $N_{\text{traj}} = 100$ and $\omega = 0.1J$ with $T = 50/J$. $Q(t)$ for all the trajectories (lines with transparent colors) and the trajectory average $Q(t)$ (black line) are shown in (a)–(c) for $\gamma = 0.2J$, $0.4J$, and $0.8J$, respectively. Similar to what we did in (a)–(c), we plot the phonon density n_{ph} in (d)–(f), respectively.

under $\hat{H}_{\text{el}}(t)$, leading to a breakdown of pumping. In this region, $E_g(t)$ is not exactly zero, which is a finite-size effect, and is expected to be zero in the thermodynamic limit. $n_{\text{dn}} \sim n_{\text{up}}$ shown in Fig. 4(f) also suggests no change in $Q(t)$ as $|\Psi(t)\rangle$ is equally mixed in both bands.

IV. OUT OF RESONANCE CONDITION

Moving away from resonance, we encounter different physical properties. In this regime, the pumping is found to be quantized at a sufficiently finite value of γ. Ultimately, with increasing γ, the TCP breaks down. We analyze the same quantities studied in the previous section to capture the physics. In Figs. 5(a)–5(c), we plot $Q(t)$ for $\gamma = 0.2J$, $0.4J$, and $0.8J$, respectively, for 100 trajectories (transparent lines) where the average $Q(t)$ over the trajectories is represented by the opaque black line. Even though the initial $\{q_i, p_i\}$ are different for different trajectories, for finite $\gamma = 0.2J$, we see quantized $Q(t)$ all the way to the 50th pump cycle, and $Q(t)$ for all the trajectories merge together, which implies a robust TCP at finite phonon coupling γ.

We observe different effects in the dynamics by increasing γ to $0.4J$. In this case, the charge pumping breaks down after a few pump cycles, and $Q(t)$ is not quantized anymore in the few initial pumping cycles that still exhibit finite pumping. For different trajectories, $Q(t)$ shows a substantial fluctuation from the average value as a result of topologically unprotected dynamics, which stems from the breakdown of TCP and largely depends on the initial conditions. Further increasing $\gamma = 0.8J$, the pumping breaks down from the beginning, and $Q(t)$ for all the trajectories shows a large fluctuation similar to the $\gamma = 0.4J$ case.

A. Quantized pumping with phonons

Unlike the resonance case where the TCP breaks down for small γ [Fig. 5(a)] at later pump cycles, in this case, TCP may remain stable at small γ. We confirm the stability by analyzing the behavior of $n_{\text{ph}}(t)$. Figures 5(d)–5(f) show $n_{\text{ph}}(t)$ for the same parameters considered in Figs. 5(a)–5(c), respectively. We see that $n_{\text{ph}}(t)$ periodically reaches zero after every few pump cycles [Fig. 5(e)] for the $\gamma = 0.2J$ case. Also, the extreme value of $n_{\text{ph}}(t)$ is comparatively smaller [compare with Fig. 2(d)]. This behavior is completely different from the resonance case where n_{ph} keeps increasing in the initial pump cycles where pumping is quantized [compare with Figs. 2(d) and 2(e)]. This regular oscillatory behavior of n_{ph} guarantees the same dynamics for further pump cycles beyond the 50th cycle, and TCP survives. In Fig. 5(f), for the first few cycles where pumping is nonzero, the trend of $n_{\text{ph}}(t)$ looks similar to the $\gamma = 0.2J$ case. However, the features look comparable to the resonance case when the pumping is absent [compare Figs. 5(f) and 2(f)].

The effective pumping path for $\gamma = 0.2J$ also suggests a robust winding, which is shown in Figs. 6(a)–6(c). We can see that the pumping path evolves similarly for different time windows and does not have any trend to collapse towards the origin, indicating robust TCP. $Q(t)$, $E_g(t)$, n_{dn}, and n_{up} are plotted in Figs. 6(d)–6(f), respectively, for this case. The finite $E_g(t)$ and $n_{\text{dn}} = 1$ ($n_{\text{up}} = 0$) at all times illustrate the adiabatic dynamics under $\hat{H}_{\text{el}}(t)$, securing the quantization of pumping.

To summarize, we observe a significant difference at small γ when comparing pumping at resonance and away from resonance. The behavior of $n_{ph}(t)$ and the effective pumping

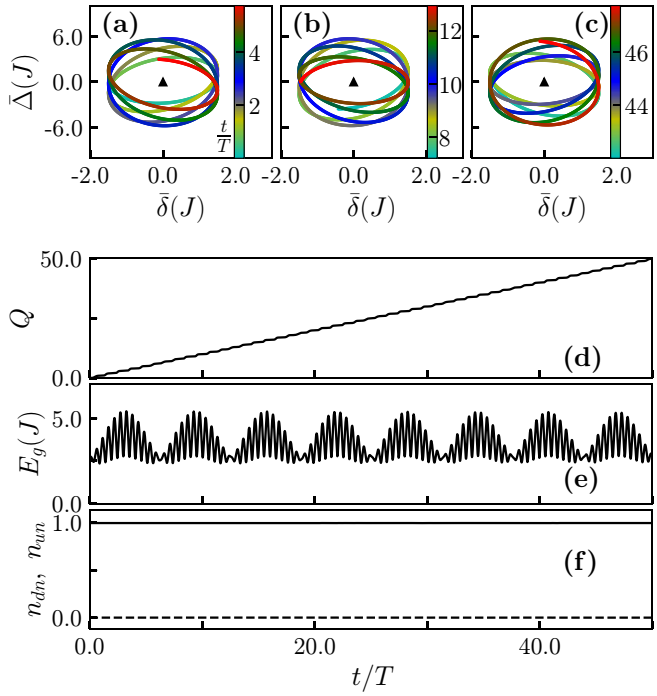

FIG. 6. Different quantities are displayed here after averaging over trajectories with $N_{\text{traj}} = 100$ to analyze the quantized pumping at finite $\gamma = 0.2J$ away from resonance where $\omega = 0.1J$ and $T = 50/J$. The effective pumping path is shown for three different time windows in (a)–(c), corresponding to Fig. 5(a), which is also shown in (d) for reference. The black triangles mark the origins where E_g should vanish. $E_g(t)$ is shown in (e), and $n_{\text{dn}}(t)$ (solid line) and $n_{\text{up}}(t)$ (dashed line) are plotted in (f).

path suggests stable pumping over the simulated time window for the out of resonance case. We stress that this does not rule out a change in behavior at very long times beyond the reach of simulations.

B. Breakdown of pumping

As mentioned above, for larger γ the TCP breaks down. To analyze the breakdown of pumping with increasing γ, we again pay attention to $E_g(t)$. We show the trajectory-averaged $Q(t)$ and $E_g(t)$ in Figs. 7(a) and 7(b), respectively, for the first four pump cycles with $T = 50/J$. Here, we consider $N_{\text{traj}} = 200$ to calculate the average. Comparing the two plots, we can see that $E_g(t)$ starts to vanish at certain times near the critical region ($\gamma \approx 0.4J$) and finally vanishes during the entire pump cycle for larger γ. The vanishing of E_g with time makes the dynamics under $\hat{H}_{\text{el}}$ nonadiabatic, and as a result, the TCP breaks down. Note that the negative charge pumping is also present in the off-resonant case [see the deep blue region of Fig. 7(a)].

V. STABILITY DIAGRAM

Until now, we have considered only two time periods of pumping ($T = \frac{2\pi}{0.1J}$ and $50/J$) in our analysis to detect the breakdown of TCP. Now we uncover this phenomenon by varying T. To this end, we perform the calculation for different γ and T for the first 50 pump cycles with $N_{\text{traj}} = 100$

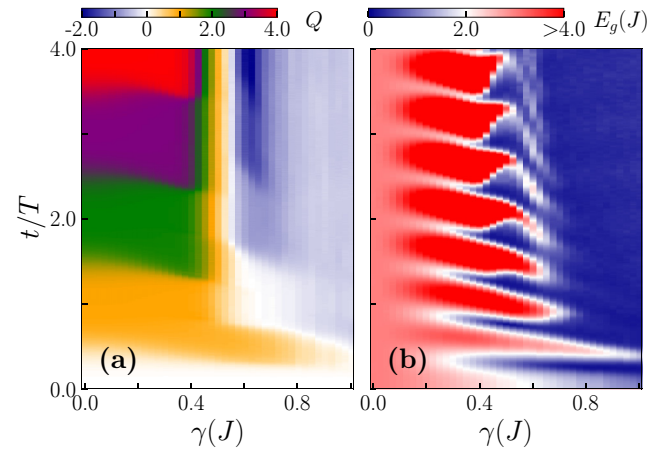

FIG. 7. (a) The trajectory-averaged $Q(t)$ and (b) $E_{\text{gap}}(t)$ are shown away from resonance with $T = 50/J$, $\omega = 0.1J$, and $N_{\text{traj}} = 200$. The breakdown of quantized pumping near $\gamma \sim 0.4J$ is portrayed.

and calculate the trajectory-averaged Q in a pump cycle by averaging the pumped charge in all the cycles. We portray the result in Fig. 8(a) as a function of γ and T, where the color bar represents the average Q in a cycle. The properties of the stability diagram are discussed below.

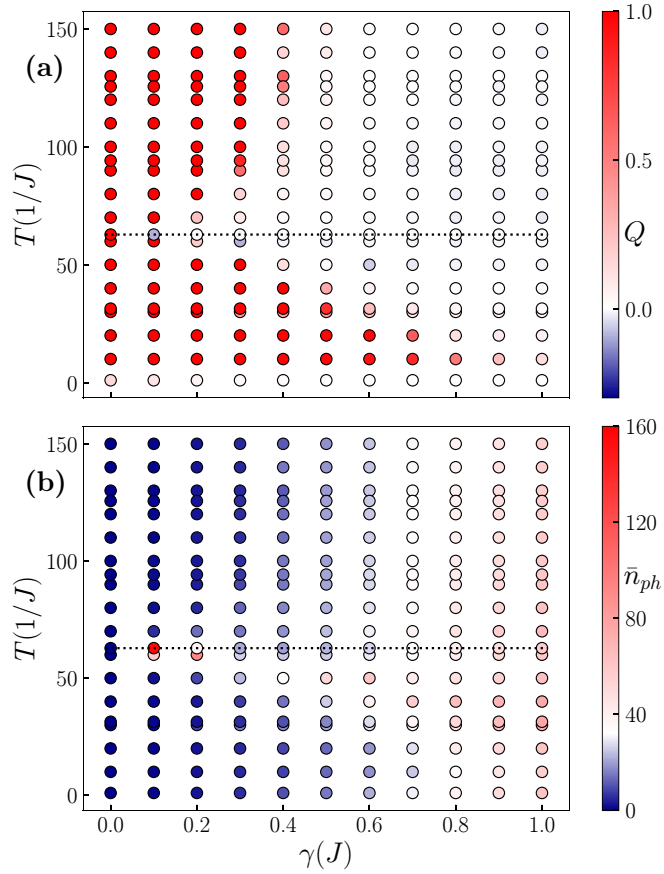

FIG. 8. Stability diagram in the T vs γ plane depending on the trajectory-averaged (a) Q in a cycle and (b) $\bar{n}_{\text{ph}}$. Here, we consider $N_{\text{traj}} = 100$ and average Q and $\bar{n}_{\text{ph}}$ over 50 pump cycles. The dashed lines represent the time period of phonons ($\frac{2\pi}{\omega}$).

In the limit of very small $T \sim 1/J$, the TCP is always absent due to a very fast pumping speed which leads to a nonadiabatic evolution. For higher values of T, the TCP breaks down after a critical γ except at resonance (marked by the dashed line), where it breaks down immediately for $\gamma > 0$. An important feature of the stability diagram is the reentrance of quantized pumping as a function of T in a certain parameter regime. For example, with $\gamma = 0.2J$, the quantization of pumping occurs in the order of a nonquantized-quantized-nonquantized-quantized manner as T increases. The reentrance of TCP with increasing T is clearly a consequence of the resonance at $T = 2\pi/\omega$. Simulations with other values of small ω exhibit qualitatively similar physical phenomena at the resonance and away from the resonance (not shown).

We also calculate the time-averaged phonon density, given by

$$\bar{n}_{\rm ph} = \frac{1}{t}\int_0^t n_{\rm ph} dt \tag{18}$$

and shown in Fig. 8(b) as a function of γ and T. Like in the previous calculation, $\bar{n}_{\rm ph}$ is averaged over $N_{\rm traj} = 100$ trajectories and 50 pump cycles. The result complements the stability diagram of Q [Fig. 8(a)] very well. We notice that the phonon excitation in the TCP region is small compared to the TCP-broken region. Around the resonance ($T = 2\pi/\omega$), marked by the dashed line, $\bar{n}_{\rm ph}$ grows faster for smaller γ, which is responsible for the early breakdown in this region.

VI. CONCLUSIONS

In conclusion, we have studied the Thouless charge pumping in the presence of optical phonons. The Rice-Mele pumping protocol extended with Holstein-like coupling to the local dispersionless phonons was used. We considered the initial conditions where the subsystems are decoupled and the phonons are in their ground state. We utilized a semiclassical approach known as the multitrajectory Ehrenfest method to analyze the system's dynamics where the electrons are treated quantum mechanically and phonon trajectories are evolved classically.

The analysis revealed a breakdown of quantized pumping induced by the phonons for any finite value of the e-ph coupling when the phonon frequency and pumping frequency match. Moreover, in this case, for smaller e-ph coupling, nonquantized positive and negative pumping is observed. The direction of pumping is accurately explained using the effective pumping path, which is the modified Rice-Mele path due to the coupling of phonon position with the electronic density. The effective pumping path was found to be winding around the origin in counterclockwise and clockwise directions for the time windows with positive and negative pumping, respectively. The nonadiabatic nature of the dynamics affects the quantization of pumping in this regime. The nonadiabaticity is visible from the gap in the energy spectrum of the instantaneous Hamiltonian. When the pumping vanishes at higher values of e-ph coupling, the effective pumping path is seen to cross the origin in every cycle during the evolution, which explains the breakdown.

When the pumping period is out of resonance, the phonon-induced breakdown of the quantized pumping still exists. Yet a parameter regime of robust quantized pumping exists before it breaks down at the larger e-ph coupling. The periodically oscillating phonon number evolution and nonshrinking stable effective pumping path signal the robustness of quantization in this case. The adiabatic nature of the pumping does not hold after the breakdown of pumping for larger e-ph coupling, which is visible from the energy spectrum of the instantaneous Hamiltonian.

We obtained a stability diagram as a function of e-ph coupling and the time period of pumping. A wide region of quantized pumping was observed in the parameter space of finite e-ph coupling. As a result of resonance, a reentrant behavior of the quantized pumping was observed where, at a fixed e-ph coupling, the quantization reappears after a breakdown near the resonance as a function of the time period of pumping.

These results lead to an avenue of further analysis worth studying. One could do a similar analysis for quantum phonons. The system could be simulated using the tDMRG method with the local basis optimization technique [59,76]. Starting the pump from different initial states may lead to interesting outcomes. One should further consider scenarios of stable quantized pumping even in the presence of phonons. A half-filled Holstein model, for instance, could host a charge density wave state [48–50], depending on parameters, with a many-body gap. One could also extend the model for the phonons with dispersion. The addition of dispersion allows the phonons to transport energy to other sites, whereas local oscillators can do that only via electrons. The sign of the dispersion may also matter as the minimum changes its position in k space from $k = 0$ to $k = \pi$ with the sign.

The numerical data plotted in the figures are partially available [80].

ACKNOWLEDGMENTS

We thank M. ten Brink for helpful discussions. This research was funded by the Deutsche Forschungsgemeinschaft (DFG, German Research Foundation) via Research Unit FOR 2414 under Project No. 277974659.

[1] D. J. Thouless, Phys. Rev. B **27**, 6083 (1983).
[2] M. Lohse, C. Schweizer, O. Zilberberg, M. Aidelsburger, and I. Bloch, Nat. Phys. **12**, 350 (2016).
[3] C. Schweizer, M. Lohse, R. Citro, and I. Bloch, Phys. Rev. Lett. **117**, 170405 (2016).
[4] S. Nakajima, T. Tomita, S. Taie, T. Ichinose, H. Ozawa, L. Wang, M. Troyer, and Y. Takahashi, Nat. Phys. **12**, 296 (2016).
[5] Y. E. Kraus, Y. Lahini, Z. Ringel, M. Verbin, and O. Zilberberg, Phys. Rev. Lett. **109**, 106402 (2012).

[6] Y. Ke, X. Qin, F. Mei, H. Zhong, Y. S. Kivshar, and C. Lee, Laser Photonics Rev. **10**, 995 (2016).

[7] A. Cerjan, M. Wang, S. Huang, K. P. Chen, and M. C. Rechtsman, Light: Sci. Appl. **9**, 178 (2020).

[8] Z. Fedorova, H. Qiu, S. Linden, and J. Kroha, Nat. Commun. **11**, 3758 (2020).

[9] P. Titum, E. Berg, M. S. Rudner, G. Refael, and N. H. Lindner, Phys. Rev. X **6**, 021013 (2016).

[10] Y. Ke, X. Qin, Y. S. Kivshar, and C. Lee, Phys. Rev. A **95**, 063630 (2017).

[11] A. Hayward, C. Schweizer, M. Lohse, M. Aidelsburger, and F. Heidrich-Meisner, Phys. Rev. B **98**, 245148 (2018).

[12] M. Nakagawa, T. Yoshida, R. Peters, and N. Kawakami, Phys. Rev. B **98**, 115147 (2018).

[13] L. Privitera, A. Russomanno, R. Citro, and G. E. Santoro, Phys. Rev. Lett. **120**, 106601 (2018).

[14] M. M. Wauters, A. Russomanno, R. Citro, G. E. Santoro, and L. Privitera, Phys. Rev. Lett. **123**, 266601 (2019).

[15] B. A. van Voorden and K. Schoutens, New J. Phys. **21**, 013026 (2019).

[16] R. Wang and Z. Song, Phys. Rev. B **100**, 184304 (2019).

[17] Y. Kuno and Y. Hatsugai, Phys. Rev. Res. **2**, 042024(R) (2020).

[18] L. Lin, Y. Ke, and C. Lee, Phys. Rev. A **101**, 023620 (2020).

[19] P. Marra and M. Nitta, Phys. Rev. Res. **2**, 042035(R) (2020).

[20] S. Greschner, S. Mondal, and T. Mishra, Phys. Rev. A **101**, 053630 (2020).

[21] A. L. C. Hayward, E. Bertok, U. Schneider, and F. Heidrich-Meisner, Phys. Rev. A **103**, 043310 (2021).

[22] S. Mondal, S. Greschner, L. Santos, and T. Mishra, Phys. Rev. A **104**, 013315 (2021).

[23] Y. Kuno and Y. Hatsugai, Phys. Rev. B **104**, 045113 (2021).

[24] E. Bertok, F. Heidrich-Meisner, and A. A. Aligia, Phys. Rev. B **106**, 045141 (2022).

[25] Q. Fu, P. Wang, Y. V. Kartashov, V. V. Konotop, and F. Ye, Phys. Rev. Lett. **128**, 154101 (2022).

[26] T. Tuloup, R. W. Bomantara, and J. Gong, arXiv:2205.10978.

[27] S. Nakajima, N. Takei, K. Sakuma, Y. Kuno, P. Marra, and Y. Takahashi, Nat. Phys. **17**, 844 (2021).

[28] A.-S. Walter, Z. Zhu, M. Gächter, J. Minguzzi, S. Roschinski, K. Sandholzer, K. Viebahn, and T. Esslinger, arXiv:2204.06561.

[29] J. E. Avron, M. Fraas, G. M. Graf, and O. Kenneth, New J. Phys. **13**, 053042 (2011).

[30] C.-E. Bardyn, M. A. Baranov, C. V. Kraus, E. Rico, A. İmamoğlu, P. Zoller, and S. Diehl, New J. Phys. **15**, 085001 (2013).

[31] O. Viyuela, A. Rivas, and M. A. Martin-Delgado, Phys. Rev. Lett. **112**, 130401 (2014).

[32] Z. Huang and D. P. Arovas, Phys. Rev. Lett. **113**, 076407 (2014).

[33] O. Viyuela, A. Rivas, and M. A. Martin-Delgado, Phys. Rev. Lett. **113**, 076408 (2014).

[34] E. P. L. van Nieuwenburg and S. D. Huber, Phys. Rev. B **90**, 075141 (2014).

[35] D. Linzner, L. Wawer, F. Grusdt, and M. Fleischhauer, Phys. Rev. B **94**, 201105(R) (2016).

[36] F. Grusdt, Phys. Rev. B **95**, 075106 (2017).

[37] C.-E. Bardyn, L. Wawer, A. Altland, M. Fleischhauer, and S. Diehl, Phys. Rev. X **8**, 011035 (2018).

[38] R. Unanyan, M. Kiefer-Emmanouilidis, and M. Fleischhauer, Phys. Rev. Lett. **125**, 215701 (2020).

[39] A. Altland, M. Fleischhauer, and S. Diehl, Phys. Rev. X **11**, 021037 (2021).

[40] O. Viyuela, A. Rivas, and M. A. Martin-Delgado, Phys. Rev. B **86**, 155140 (2012).

[41] A. Rivas, O. Viyuela, and M. A. Martin-Delgado, Phys. Rev. B **88**, 155141 (2013).

[42] Y. He and C.-C. Chien, Phys. Rev. B **106**, 024310 (2022).

[43] Y. Vinkler-Aviv and A. Rosch, Phys. Rev. X **8**, 031032 (2018).

[44] G. Goldstein and C. Chamon, Phys. Rev. B **84**, 205109 (2011).

[45] C. Knapp, T. Karzig, R. M. Lutchyn, and C. Nayak, Phys. Rev. B **97**, 125404 (2018).

[46] P. P. Aseev, P. Marra, P. Stano, J. Klinovaja, and D. Loss, Phys. Rev. B **99**, 205435 (2019).

[47] H. Fröhlich, Adv. Phys. **3**, 325 (1954).

[48] J. E. Hirsch and E. Fradkin, Phys. Rev. B **27**, 4302 (1983).

[49] R. H. McKenzie, C. J. Hamer, and D. W. Murray, Phys. Rev. B **53**, 9676 (1996).

[50] R. J. Bursill, R. H. McKenzie, and C. J. Hamer, Phys. Rev. Lett. **80**, 5607 (1998).

[51] A. Altland and B. D. Simons, *Condensed Matter Field Theory* (Cambridge University Press, Cambridge, 2010).

[52] D. Emin, in *Polarons* (Cambridge University Press, Cambridge, 2012), pp. 86–94.

[53] F. Hébert, B. Xiao, V. G. Rousseau, R. T. Scalettar, and G. G. Batrouni, Phys. Rev. B **99**, 075108 (2019).

[54] H. Matsueda, S. Sota, T. Tohyama, and S. Maekawa, J. Phys. Soc. Jpn. **81**, 013701 (2012).

[55] G. De Filippis, V. Cataudella, E. A. Nowadnick, T. P. Devereaux, A. S. Mishchenko, and N. Nagaosa, Phys. Rev. Lett. **109**, 176402 (2012).

[56] F. Dorfner, L. Vidmar, C. Brockt, E. Jeckelmann, and F. Heidrich-Meisner, Phys. Rev. B **91**, 104302 (2015).

[57] H. Hashimoto and S. Ishihara, Phys. Rev. B **96**, 035154 (2017).

[58] Z. Huang, M. Hoshina, H. Ishihara, and Y. Zhao, Ann. Phys. (Berlin, Ger.) **531**, 1800303 (2019).

[59] J. Stolpp, J. Herbrych, F. Dorfner, E. Dagotto, and F. Heidrich-Meisner, Phys. Rev. B **101**, 035134 (2020).

[60] D. Jansen, C. Jooss, and F. Heidrich-Meisner, Phys. Rev. B **104**, 195116 (2021).

[61] Z. Huang, A. D. Somoza, C. Peng, J. Huang, M. Bo, C. Yao, J. Li, and G. Long, New J. Phys. **23**, 123020 (2021).

[62] J. Kogoj, L. Vidmar, M. Mierzejewski, S. A. Trugman, and J. Bonča, Phys. Rev. B **94**, 014304 (2016).

[63] L. Vidmar, J. Bonča, M. Mierzejewski, P. Prelovšek, and S. A. Trugman, Phys. Rev. B **83**, 134301 (2011).

[64] G. Li, B. Movaghar, A. Nitzan, and M. A. Ratner, J. Chem. Phys. **138**, 044112 (2013).

[65] P. Werner and M. Eckstein, Europhys. Lett. **109**, 37002 (2015).

[66] Z. Huang, L. Chen, N. Zhou, and Y. Zhao, Ann. Phys. (Berlin, Ger.) **529**, 1600367 (2017).

[67] L.-C. Ku and S. A. Trugman, Phys. Rev. B **75**, 014307 (2007).

[68] D. Golež, J. Bonča, L. Vidmar, and S. A. Trugman, Phys. Rev. Lett. **109**, 236402 (2012).

[69] T. Holstein, Ann. Phys. (NY) **8**, 325 (1959).

[70] M. J. Rice and E. J. Mele, Phys. Rev. Lett. **49**, 1455 (1982).
[71] P. Ehrenfest, Z. Phys. **45**, 455 (1927).
[72] J. C. Tully, Faraday Discuss. **110**, 407 (1998).
[73] A. Kirrander and M. Vacher, in *Quantum Chemistry and Dynamics of Excited States* (Wiley, Hoboken, NJ, 2020), Chap. 15, pp. 469–497.
[74] M. ten Brink, S. Gräber, M. Hopjan, D. Jansen, J. Stolpp, F. Heidrich-Meisner, and P. E. Blöchl, J. Chem. Phys. **156**, 234109 (2022).
[75] W. P. Su, J. R. Schrieffer, and A. J. Heeger, Phys. Rev. Lett. **42**, 1698 (1979).
[76] C. Brockt, F. Dorfner, L. Vidmar, F. Heidrich-Meisner, and E. Jeckelmann, Phys. Rev. B **92**, 241106(R) (2015).
[77] S. R. Manmana, A. Muramatsu, and R. M. Noack, in Lectures on the Physics of Highly Correlated Electron Systems IX: *Ninth Training Course in the Physics of Correlated Electron Systems and High-T_c Superconductors*, AIP Conf. Proc. No. 789 (Melville, NY, 2005), pp. 269.
[78] G. Vidal, Phys. Rev. Lett. **93**, 040502 (2004).
[79] U. Schollwöck, Ann. Phys. (NY) **326**, 96 (2011).
[80] S. Mondal, E. Bertok, and F. Heidrich-Meisner, arXiv:2209.06124.